Electron capture in collisions of Si^{3+} ions with atomic hydrogen from low to intermediate energies

C. H. Liu,[1] L. Liu,[2] and J. G. Wang[2]

[1]*Institute of Modern Physics, Chinese Academy of Sciences, Lanzhou 730000, People's Republic of China*

[2]*Data Center for High Energy Density Matter, Institute of Applied Physics and Computational Mathematics, P.O. Box 8009, Beijing 100088, People's Republic of China*

(Received 28 April 2014; published 22 July 2014)

The electron capture process for the $Si^{3+}(3s) + H(1s)$ collisions is investigated by the quantum-mechanical molecular orbital close-coupling (MOCC) method and by the two-center atomic orbital close-coupling (AOCC) method in the energy range of 10^{-5}–10 keV/u and 0.8–200 keV/u, respectively. Total and state-selective cross sections are presented and compared with the available theoretical and experimental results. The present MOCC and AOCC results agree well with the experimental measurements, but show some discrepancy with the calculations of Wang *et al.* [Phys. Rev. A **74**, 052709 (2006)] at $E > 40$ eV/u because of the inclusion of rotational couplings, which play important roles in the electron capture process. At lower energies, the present results are about three to five times smaller than those of Wang *et al.* due to the difference in the molecular data at large internuclear distances. The energy behaviors of the electron capture cross sections are discussed on the basis of identified reaction mechanisms.

DOI: 10.1103/PhysRevA.90.012708 PACS number(s): 34.70.+e, 34.20.−b

I. INTRODUCTION

Electron capture in multicharged ion and neutral atom collisions has attracted extensive theoretical and experimental attention, due to their diverse applications in laboratory plasmas and astrophysics [1]. In the edge and divertor regions of magnetically confined plasma, electron capture of multiply charged impurity ions with atomic hydrogen influences the ionization balance and plasma cooling [2,3]. In astrophysics, charge transfer plays an important role in determining the properties of the observed gas [4]. The extreme ultraviolet (EUV) and x-ray emission from comets and planetary atmospheres have been explained by charge transfer of heavy solar wind ions, including Si^{q+}, with neutral species in the cometary and planetary atmosphere [5]. In order to simulate the behavior of the relevant environments, accurate total and state-selective capture cross sections are essential.

For the $Si^{3+} + H$ collisions, at energies below 10 eV/u, Herrero *et al.* [6] estimated the total single-electron capture cross sections by the Landau-Zener (LZ) method with *ab initio* parameters. Wang *et al.* [7] calculated the charge transfer cross sections in a wide energy range of 10^{-5}–10^{3} keV/u by using two theoretical methods: the classical trajectory Monte Carlo (CTMC) method and the quantum-mechanical molecular orbital close-coupling (MOCC) method. The MOCC calculations utilize the *ab initio* adiabatic potentials and nonadiabatic radial coupling matrix elements obtained from the work of Herrero *et al.* [6] with two effective electrons. Their CTMC results agree well with the experimental measurements of Kim *et al.* [8] for energies from 50 to 150 keV/u, and the MOCC results are about 1.5 times smaller than the LZ results of Herrero *et al.* [6]. Bruhns *et al.* [9] performed absolute cross-section measurements for $Si^{3+} + H$ collisions in the energy range between 44 and 2444 eV/u using the upgraded ion-atom merged-beam apparatus. The experimental electron capture cross sections are larger than the MOCC calculations of Wang *et al.* [7] at energies higher than 0.5 keV/u, but smaller at $E < 0.1$ keV/u. We note that in the MOCC calculations of Wang *et al.* [7], a small molecular basis is used and the rotational coupling is not included. The electron translational factors (ETFs), which would have important effect at energies above 1 keV/u, were also neglected in the MOCC calculations of Ref. [7]. Recently, Guevara *et al.* [10] investigated the $Si^{3+} + H$ collision in the energy range of 0.04–10 keV/u using the electron nuclear dynamics (END) method, in which all electrons in the wave function are considered and the nuclear trajectories are described classically. Their charge transfer cross sections are larger than the MOCC results of Wang *et al.* [7] by a constant difference of 2–3 $\times$ 10^{-16} cm^2 over the energy range of 0.04–1 keV/u. The energy dependences of both the MOCC and END results are different from the experimental measurements of Bruhns *et al.* [9]. The experimental results [9] are closer to the MOCC calculations [7] for $E < 0.3$ keV/u but remain closer to the END results [10] for higher energies.

In order to clarify the discrepancies between the experimental and theoretical results, in the present work, we shall study the electron capture process for the $Si^{3+} + H$ collision by using the quantum-mechanical MOCC method [11,12] in the energy range of 0.01 eV/u–10 keV/u with a large molecular basis. Besides the radial couplings, in our calculations we also included the rotational couplings, which were not considered in the MOCC calculations of Wang *et al.* [7] and may play important roles for electron capture. The molecular structure data (potential curves and radial and rotational coupling matrix elements) required in the calculations will be determined by using the multireference single- and double-excitation configuration interaction (MRDCI) method [13,14] with Gaussian-type basis set. The atomic orbital close-coupling (AOCC) method will also be used in the intermediate energy range of 0.8–200 keV/u.

Atomic units will be employed throughout, unless explicitly indicated otherwise.

 ©2014 American Physical Society

II. COMPUTATIONAL METHOD

A. Molecular structure

The MRDCI package [13,14] was employed to calculate the potential energy curves and the radial and rotational coupling matrix elements. The correlation-consistent, polarization valence, quadruple-ζ (cc-pVQZ) type basis set [15] was employed for Si and H atoms, but the g-type basis was discarded. Besides the above basis set, the diffuse $(1s1p1d)$ basis was added for the Si atoms. A threshold of 10^{-8} hartrees was used to select the configurations at the internuclear distances of 1–30 a.u. Using the obtained electronic wave functions, the radial and rotational coupling matrix elements were calculated by the finite differentiation method [16] and analytical approaches, respectively.

In the present calculations, the electron translational effect was included by transforming the radial and rotational coupling matrix elements between states ψ_K and ψ_L into [17]

$$\begin{aligned} &\langle\psi_K|\,\partial/\partial R - (\varepsilon_K - \varepsilon_L)z^2/2R\,|\psi_L\rangle\,, \\ &\langle\psi_K|\,iL_y + (\varepsilon_K - \varepsilon_L)zx\,|\psi_L\rangle\,, \end{aligned} \tag{1}$$

where ε_K and ε_L are the electronic energies of ψ_K and ψ_L states, and z^2 and zx are the components of the quadrupole moment tensor. Equation (1) is deduced by introducing appropriate reaction coordinates [11,18], originally developed by Thorson and Delos [19] and Mittleman [20]. The modification is similar in form to that resulting from the common translation factor method [21].

B. MOCC method

Details of the quantum-mechanical MOCC method for ion-atom collisions can be found elsewhere [11,12] and only the basic technique is outlined here. In our MOCC method, the log-derivative method of Johnson [22] was employed to solve a coupled set of second-order differential equations. Transitions between channels are driven by radial and rotational (A^r and A^θ) couplings of the vector potential $\vec{A}(\vec{R})$, where $\vec{R}$ is the internuclear distance vector. In order to avoid the numerical difficulties encountered in the integration of the radial coupled equations based on the adiabatic representation, the diabatic transformation [12,23] was adopted for electronic states. The radial functions are matched to the plane-wave and Coulomb boundary conditions for neutral and Coulomb channels, respectively. The cross section for electron transition from channel α to channel β can be expressed by the S matrix

$$\sigma_{\alpha\to\beta} = \frac{\pi}{k_\alpha^2}\sum_J (2J+1)\left|\delta_{\alpha\beta} - S^J_{\alpha\beta}\right|^2, \tag{2}$$

where k_α is the initial momentum in the center-of-mass coordinate and J is the total angular momentum quantum number.

C. AOCC method

The details of the two-center AOCC methods can be found in the literature [11,24] and here we only present its brief account. The total electron wave function can be expanded in terms of bound atomic orbitals of the two ionic centers, (ϕ^A, ϕ^B), multiplied by plane-wave ETFs,

$$\Psi(\vec{r},t) = \sum_i a_i(t)\phi_i^A(\vec{r},t) + \sum_j b_j(t)\phi_j^B(\vec{r},t). \tag{3}$$

The frozen core approximation is employed for the $Si^{3+}(3s)$ ion. The interaction of the Si^{3+} ion with the electron initially resident on H is represented by the one-electron model potential [7]. The straight-line approximation is adopted for nuclear motion. The substitution of the expansion (3) into the time-dependent Schrödinger equation gives the first-order coupled equations for the amplitudes $a_i(t)$ and $b_j(t)$:

$$\begin{aligned} i(\dot{A} + S\dot{B}) &= HA + KB, \\ i(\dot{B} + S^\dagger\dot{A}) &= \bar{K}A + \bar{H}B, \end{aligned} \tag{4}$$

where A and B are the vectors of the amplitudes a_i and b_j, respectively. S is the overlap matrix ($S^\dagger$ is its transposed form), H, $\bar{H}$ and K, $\bar{K}$ are the direct and exchange coupling matrices. The cross section for electron capture is obtained by integration of corresponding probabilities over the impact parameter b:

$$\sigma_{cx,j} = 2\pi\int_0^\infty |b_j(+\infty)|^2 bdb. \tag{5}$$

III. RESULTS AND DISCUSSIONS

A. Adiabatic potentials and couplings

Using the MRDCI method, we calculated the lowest sixteen singlet states and twelve triplet states, which correlate to the lowest nine $^1\Sigma$, two $^1\Delta$, five $^1\Pi$ states, and six $^3\Sigma$, one $^3\Delta$, five $^3\Pi$ states of the SiH^{3+} molecule, respectively. All of the twelve electrons are considered in our calculation. In Table I, the asymptotic energy of a few lowest states in the present calculation are compared with the experimental atomic

TABLE I. Asymptotic separated-atom energies of SiH^{3+} molecule.

		Energy (eV)				
Molecular state	Asymptotic atomic state	Expt. [25]	Theor. [6]	Error [6]	Theor.	Error
$1\,^1\Sigma$	$Si^{2+}(3s^2)[^1S] + H^+$	−19.895	−19.843	0.052	−19.784	0.111
$2\,^1\Sigma$, $1\,^1\Pi$	$Si^{2+}(3s3p)[^1P] + H^+$	−9.618	−9.421	0.197	−9.503	0.115
$3\,^1\Sigma$, $2\,^1\Pi$	$Si^{2+}(3p^2)[^1D] + H^+$	−4.742	−4.804	−0.062	−4.725	0.017
$1\,^3\Sigma$, $1\,^3\Pi$	$Si^{2+}(3s3p)[^3P] + H^+$	−13.325	−13.364	−0.039	−13.314	0.011
$2\,^3\Pi$	$Si^{2+}(3p^2)[^3P] + H^+$	−3.780	−3.745	0.035	−3.791	−0.011
$4\,^1\Sigma$, $2\,^3\Sigma$	$Si^{3+}(3s) + H(1s)$	0	0	0	0	0

TABLE II. Position R_0 and energy separation H_{12} of the avoided crossing between the $3\,^1\Sigma$ and $4\,^1\Sigma$ states.

$3\,^1\Sigma$-$4\,^1\Sigma$	Present	Herrero *et al.* [6]	Butler and Dalgarno [26]
R_0 (a.u.)	11.45	11.29	11.6
H_{12} (a.u.)	0.00084	0.00056	0.00063

energies [25] and the calculations of Herrero *et al.* [6]. These states would play dominant roles for the electron capture process of Si^{3+} + H collision. The errors of our calculated energies with respect to the experimental atomic energies are less than 0.12 eV in the asymptotic region. We can see that except for the $Si^{2+}(3s^2)$ + H^+ state, our calculated energies agree better with the experimental results [25] than the calculations of Ref. [6].

The adiabatic potential curves for the singlet and triplet molecular states of SiH^{3+} are shown in Figs. 1(a) and 1(b), respectively, for the internuclear distances R = 0–30 a.u. The $4\,^1\Sigma$ and $2\,^3\Sigma$ states represent the initial channels of $Si^{3+}(3s)$ + H collisions. For singlet states, the avoided crossing at 11.45 a.u. between the initial $4\,^1\Sigma$ state and the $3\,^1\Sigma$ state [asymptotically correlating to $Si^{2+}(2p^2\ [^2D])$ + H^+ state] would be important at very low energies. In Table II, the position and energy separation of this avoided crossing are compared with those in Refs. [6,26]. These parameters would sensitively influence the $Si^{2+}(2p^2\ [^2D])$ capture cross sections in the very-low-energy region. From Table I we know that the present calculated asymptotic energy of the $Si^{2+}(2p^2\ [^2D])$ + H^+ state agree better than the calculation of Ref. [6] with the experimental result. The precise asymptotic energy is necessary for the accurate calculation of the capture cross sections. At high energies, this avoided crossing can be treated as diabatic. The radial and rotational couplings between the $3\,^1\Sigma$ state with the $2\,^1\Sigma$ and $1\,^1\Pi$ states would influence the electron capture process effectively. The upper states and the lowest $1\,^1\Sigma$ state would not influence the charge transfer obviously. For triplet states, it can be seen that there is no effective coupling appearing between the initial $2\,^3\Sigma$ state and other states.

Figures 2(a) and 2(b) show the radial coupling matrix elements between the lowest few states for singlet and triplet manifolds, respectively, with the electron translational effects included. Correlating to the strong avoided crossing between the $4\,^1\Sigma$ and $3\,^1\Sigma$ states, a sharply peaked Landau-Zener coupling appears at R = 11.45 a.u. This coupling will only take effect in the very-low-energy region. Besides this coupling, there are strong Demkov couplings between $2\,^1\Sigma$ and $3\,^1\Sigma$ states at about 6.2 and 3.3 a.u. These couplings will effectively populate the system to the $2\,^1\Sigma$ state, which asymptotically correlates to the $Si^{2+}(3s3p)$ + H^+ state. The $3\,^1\Sigma$–$4\,^1\Sigma$ couplings at 2.2 and 4.2 a.u. will promote the system to the $Si^{2+}(2p^2\ [^2D])$ + H^+ state at high energies. The $4\,^1\Sigma$-$5\,^1\Sigma$ coupling at 3–5 a.u. and the couplings correlating with the series of $5\,^1\Sigma$-$6\,^1\Sigma$-$7\,^1\Sigma$-$8\,^1\Sigma$-$9\,^1\Sigma$ avoided crossings at 2.5–8.5 a.u. [see Fig. 1(a)] will populate the high states in the receding stage of the collision. For triplet states, no effective radial coupling is found between the entrance $2\,^3\Sigma$ channel and other states. The weak $1\,^3\Sigma$-$2\,^3\Sigma$ coupling at about 5 a.u. would play the dominant role for charge transfer in triplet manifold and populate the $Si^{2+}(3s3p)$ state. The $2\,^3\Sigma$-$3\,^3\Sigma$ coupling at about 3 a.u. and the series of $3\,^3\Sigma$-$4\,^3\Sigma$-$5\,^3\Sigma$-$6\,^3\Sigma$ couplings at 2.5–8 a.u. will promote the system to high states.

In Figs. 3(a) and 3(b) we show some important rotational couplings for the singlet and triplet molecular states, respectively. The $2\,^1\Sigma$-$1\,^1\Pi$, $3\,^1\Sigma$-$2\,^1\Pi$, and $1\,^3\Sigma$-$1\,^3\Pi$ rotational couplings are between states converging to the same configurations and asymptotically converge to a particularly large constant. These couplings obviously play prominent roles in the rearrangement of the system between states with the same principal and angular quantum number in the receding stage. The magnitudes of the $3\,^1\Sigma$-$2\,^1\Pi$ and $4\,^1\Sigma$-$2\,^1\Pi$ rotational couplings were exchanged with each other at R = 11.45 a.u. This is because that the main configuration of the $3\,^1\Sigma$ state was exchanged with that of the $4\,^1\Sigma$ state at the strong anticrossing point. At $R > 11.45$ a.u., the $4\,^1\Sigma$ state represent the entrance channel of $Si^{3+}(3s)$ + H(1s), but at $R < 11.45$ a.u., the main configuration of $3\,^1\Sigma$ state becomes $Si^{3+}(3s)$ + H(1s). The $3\,^1\Sigma$ state is strongly rotationally coupled with the $1\,^1\Pi$ state at about 5 a.u. This coupling will promote the system to populate the $Si^{2+}(3s3p)$ + H^+ state. The $3\,^1\Sigma$ state is also strongly coupled with the $2\,^1\Pi$ states at very small internuclear distance. This coupling would populate the $Si^{2+}(2p^2\ [^2D])$ + H^+ state at high-energy region. For triplet

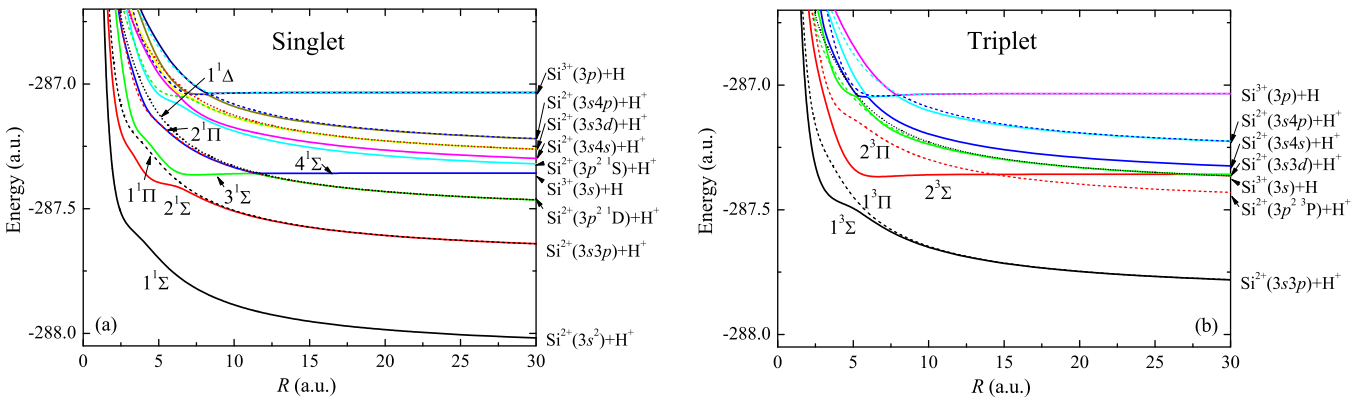

FIG. 1. (Color online) Adiabatic potential curves for SiH^{3+}. The solid lines, dotted lines, and dashed lines represent the Σ, Π, and Δ states, respectively. (a) Singlet states; (b) triplet states.

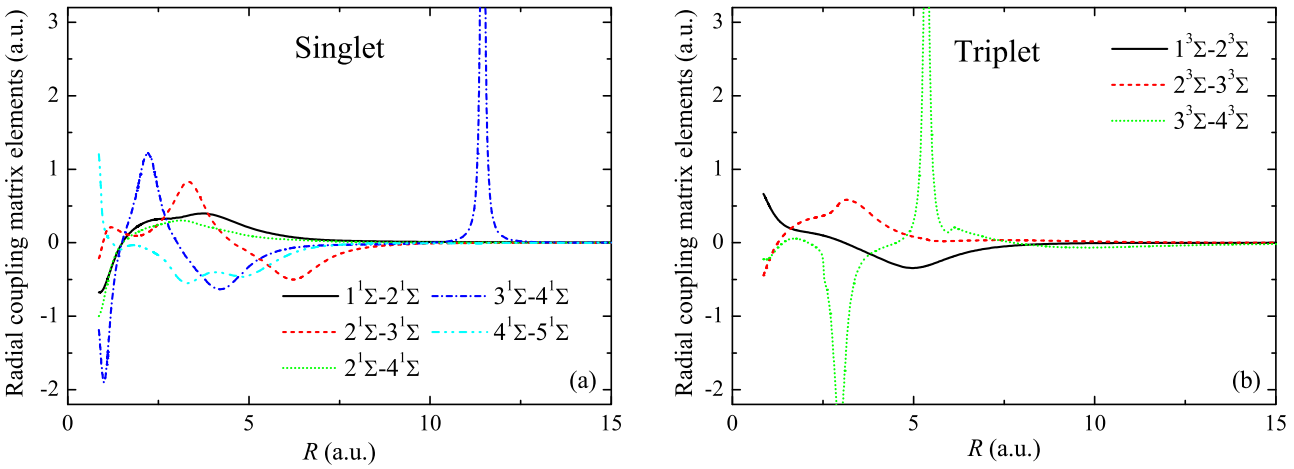

FIG. 2. (Color online) Radial coupling matrix elements for SiH^{3+}. (a) Singlet states; (b) triplet states.

states, there is no strong rotational coupling between the initial $2\,^3\Sigma$ state and $^3\Pi$ states appearing at $R > 2.5$ a.u. The weak $2\,^3\Sigma$-$1\,^3\Pi$ coupling at about 4 a.u. would promote the system to the $Si^{2+}(3s3p) + H^+$ state.

B. Electron capture cross sections

The electron capture cross sections of $Si^{3+}(3s) + H(1s)$ collision were calculated by the MOCC and AOCC method in the energy range of 10^{-5}–10 keV/u and 0.8–200 keV/u, respectively. In our MOCC calculation, we included all 28 channels shown in Fig. 1, which are nine $^1\Sigma$, five $^1\Pi$, and two $^1\Delta$ states in the singlet manifold and six $^3\Sigma$, five $^3\Pi$, and $1\,^3\Delta$ states in the triplet manifold. The values of R_{max} for matching the boundary conditions were chosen from 2000 to 200 a.u. for collision energies varying from 10^{-5} to 10 keV/u. Beyond $R = 30$ a.u., the potentials of the initial $4\,^1\Sigma$ and $2\,^3\Sigma$ states as well as the Si^{3+} excitation channels were extended to larger internuclear distances by the dipole polarization potential $V_{pol}(R) = -\alpha_d/2R^4$, where $\alpha_d = 4.5$ a.u. is the dipole polarizability of the H(1s) atom. The long-range asymptotic behavior of the charge transfer final states was described by the Coulomb form. Because the singlet and triplet manifolds do not couple with each other in the nonrelativistic approximation, the MOCC calculations were performed separately for each manifold. The total and state-selective cross sections were averaged over the statistical weights of 1/4 for the singlet and 3/4 for the triplet results. In our AOCC calculation, the expansion basis includes all states on the ionic $Si^{3+}(3s)$ center with the principal quantum number $n \leqslant 7$. Because the single-electron approximation was considered, the $Si^{2+}(2p^2)$ states were not involved.

The total electron capture cross sections for the $Si^{3+} + H$ collision are displayed in Fig. 4 in the energy range of 10^{-5}–200 keV/u. The present MOCC and AOCC results are compared with the MOCC and CTMC results of Wang *et al.* [7], the END results of Guevara *et al.* [10], the LZ calculations of Herrero *et al.* [6], and the experimental measurements of Bruhns *et al.* [9] and Kim *et al.* [8]. The present AOCC calculations agree very well with the experimental measurements of Kim *et al.* [8] at about 100 and 150 keV/u. At lower energies, the magnitudes of the AOCC results are a little smaller than the experimental results in Ref. [8]. The CTMC results of Wang *et al.* [7] are a little larger than the present AOCC results at $E > 40$ keV/u, but become smaller than the AOCC calculations in the lower-energy region, where the

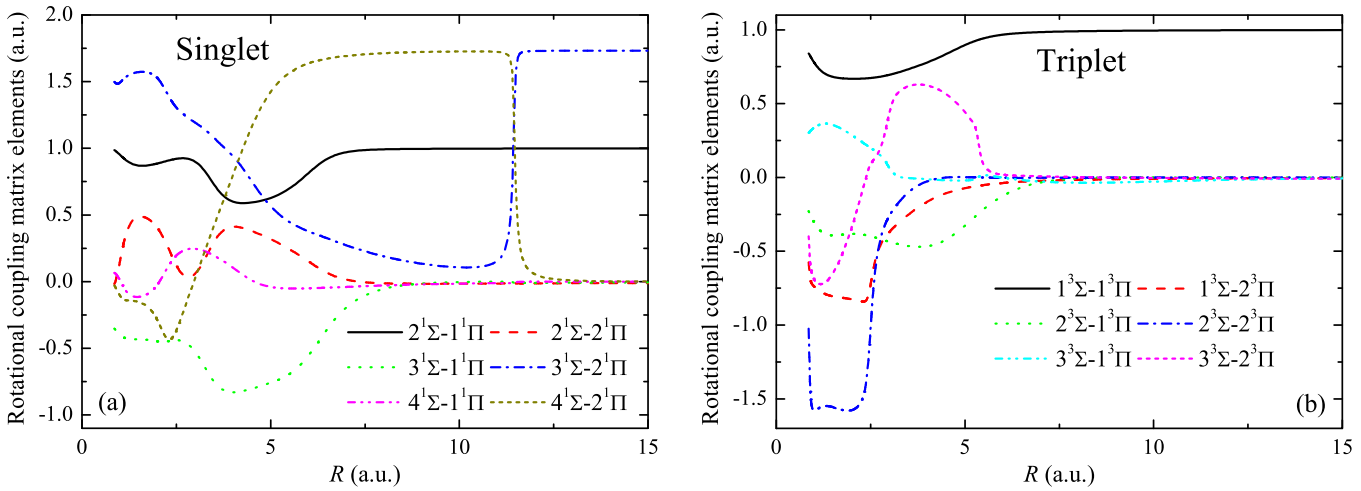

FIG. 3. (Color online) Rotational coupling matrix elements for BeH^{3+}. (a) Singlet states; (b) triplet states.

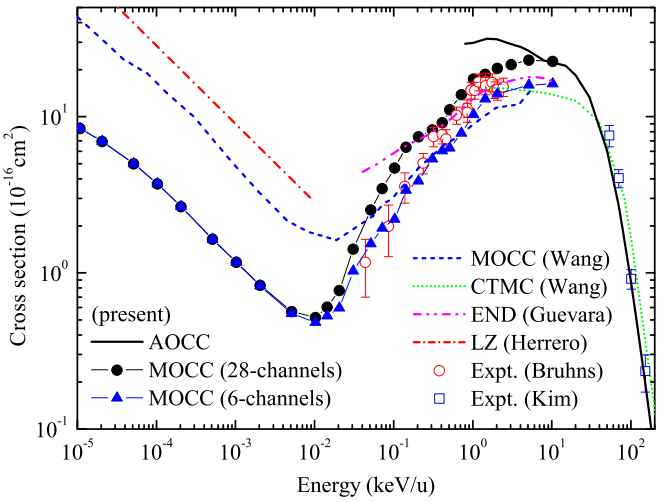

FIG. 4. (Color online) Total electron capture cross sections for the $Si^{3+} + H$ collisions. Present 28-channel MOCC calculation: filled circles; present six-channel MOCC calculation: filled angles; present AOCC calculation: solid line; MOCC results of Wang *et al.* [7]: dashed line; CTMC results of Wang *et al.* [7]: dotted line; END results of Guevara *et al.* [10]: dash-dot-dotted line; LZ results of Herrero *et al.* [6]: dash-dotted line; the experimental measurement of Bruhns *et al.* [9]: open circles; the experimental results of Kim *et al.* [8]: open squares.

CTMC method is known to be inappropriate [11]. Our AOCC results show good mutual agreement with the 28-channel MOCC result at 10 keV/u. At lower energies, the AOCC results tend to increase with the decreasing of energy, while our MOCC results slowly decrease with decreasing energy in the keV region. This is because the single-electron approximation is used in the present AOCC calculations, and the $Si^{2+}(3p^2)$ states are not involved, so that the AOCC results are inaccurate in the keV region.

The present MOCC results agree well with the experimental measurements of Bruhns *et al.* [9] in the energy range 0.3–2 keV/u, and are somewhat larger than the experimental measurements at energies below 0.3 keV/u. The smaller experimental cross sections of [9] at low energies may be due to the loss of collected signal. Bruhns *et al.* [9] stated that the signal-to-background ratio was insufficient to collect statistically significant data at energies below 44 eV/u. The inadequate angular collection may be another reason for the loss of signal in the low-energy region, where the large-angle scattering should play an important role. Our MOCC results are larger than the MOCC calculations of Wang *et al.* [7] at energies above 0.04 keV/u, but become smaller than those of Ref. [7] at lower energies. We note that in the calculations of Wang *et al.* [7], the rotational couplings are not involved, and only the lowest four $^1\Sigma$ states and two $^3\Sigma$ states are included. We also did similar calculations by using the same molecular basis. The results are also shown in Fig. 4 and indicated by six channels. We can see that the six-channel results are closer to the results of Wang *et al.* at energies above 0.05 keV/u, but at lower energies, the six-channel results decrease rapidly and tend to be close to the 28-channel results. The difference of the present calculations with those of Wang *et al.* [7] arises from the different molecular data. Although our six-channel results appear to agree better with the experimental measurements [9] than the 28-channel calculations, we think that the six-channel results are inaccurate because the rotational couplings cannot be ignored as we have concluded from the molecular data (see Figs. 1–3). When we included the six channels as well as the $1,2\,^{1,3}\Pi$ states in the calculations, the cross sections are similar to the present 28-channel results. The END results of Guevara *et al.* [10] are somewhat smaller than the present MOCC results at $E > 0.4$ keV/u and also show good agreement with the experiments [9]. At lower energies, their results slowly decrease and deviate from the experiment results [9]. The reason may be that in the END calculations, the classical treatment is adopted for the nuclear trajectories.

At $E < 5$ eV/u, the cross sections increase with decreasing energy due to the sharp $3\,^1\Sigma$-$4\,^1\Sigma$ radial coupling at $R = 11.45$ a.u. The present results are about three to five times smaller than those of Wang *et al.* [7]. The LZ results of Herrero *et al.* [6] are even larger than the MOCC results of Ref. [7]. As we have pointed out in Table II the position and energy separations of the $3\,^1\Sigma$-$4\,^1\Sigma$ avoided crossing in the present calculations are different from those of Ref. [6]. In the MOCC calculation of Wang *et al.* [7], the molecular data in Ref. [6] are used. From Table I we know that the present asymptotic energy of the $Si^{2+}(3p^2[^1D]) + H^+$ state is closer to the experimental one than that in Ref. [6]. The precise molecular data in the present calculation would guarantee the more accurate cross-section results.

The state-selective cross sections were calculated by the MOCC and AOCC methods. In Fig. 5, our results for electron capture to $3s^2$, $3p^2$, $3s3p$, $3s3d$ shells of the Si^{2+} ion are compared with the MOCC and CTMC calculations of Wang *et al.* [7]. At energies higher than 20 eV/u, the $3s3p$ state plays the dominant role for the electron capture process. This is because both the initial singlet and triplet states have relatively strong radial and rotational couplings with the $3s3p$ states at about 5 a.u. At $E > 20$ keV/u, the $3s3d$ state also becomes an important capture channel because it has three compositions. The $3p^2$ cross sections begin to increase with the decreasing of energy at $E < 30$ eV/u and the $3p^2$ state becomes the dominant capture channel at $E < 10$ eV/u. This is because the sharp $3\,^1\Sigma$-$4\,^1\Sigma$ radial coupling at $R = 11.45$ a.u. begins to take effect. The present MOCC results for the dominant $3s3p$ channels agree well with the AOCC calculations at 5–10 keV/u. Due to the single-electron approximation used in the present AOCC calculation, the $3p^2$ state cannot be included in the calculations, and the relatively small $3s^2$ and $3s3d$ cross sections of our MOCC and AOCC calculations do not agree well with each other. Because the Π and Δ states are not included in the MOCC calculations of Ref. [7], their results are somewhat smaller than the present calculations at $E > 20$ eV/u for the $3s3p$ state and at $E > 0.5$ keV/u for the $3p^2$ state. At lower energies, the asymptotic energy level would play an important role in the electron capture process. The $3\,^1\Sigma$-$4\,^1\Sigma$ avoided crossing in Refs. [6,7] appears at a relatively smaller R than the present calculations (see Table II); their $3p^2$ cross sections begin to increase at a higher energy and the numerical values are larger than the present calculations at $E < 0.1$ keV/u. In Ref. [7], because of the small molecular basis used in the MOCC calculation, the relatively small results

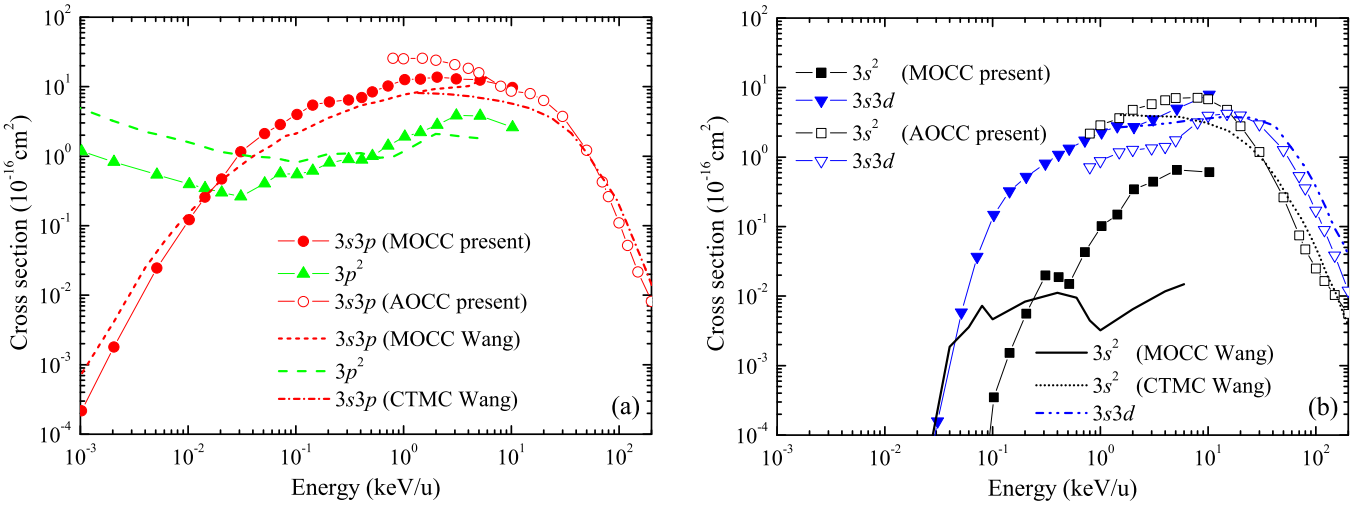

FIG. 5. (Color online) State-selective cross sections for electron capture to $3p^2$, $3s3p$ states (a) and $3s^2$, $3s3d$ states (b) of the Si^{2+} ions for Si^{3+} + H collision. The present MOCC and AOCC results are compared with the MOCC and CTMC results of Wang *et al.* [7].

of the $3s^2$ channel would be not exactly correct and the $3s3d$ state is not involved.

Figure 6 shows the state-selective cross sections for electron capture to the $3s4l$ shells of the Si^{2+} ion. In the present MOCC calculations, the $3s4d$ and $3s4f$ states were not included. The capture cross sections of each $3s4l$ state would be not so exact. In Fig. 6 we only give the total $n = 4$ results for electron capture to the $Si^{2+}(3snl)$ states of the MOCC calculation. The present MOCC and AOCC results for total $n = 4$ capture show good mutual agreement with each other in the overlapping energy range. The present AOCC results are mainly a little smaller than the CTMC results of Wang *et al.* [7]. In the present AOCC calculations, all of the $3snl$ ($n \leqslant 7$) states were involved. By comparing with the experimental results of Kim *et al.* [8] (see Fig. 4), we can believe that the present AOCC results would be more precise than the CTMC calculations [7].

In Figs. 7(a) and 7(b), we show the state-selective cross sections of our MOCC calculations for singlet and triplet

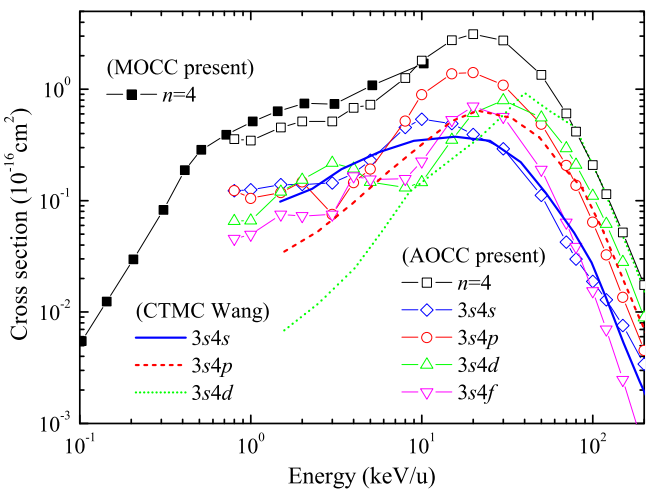

FIG. 6. (Color online) State-selective cross sections for electron capture to $3s4l$ states of Si^{2+} ions for Si^{3+} + H collision. The present MOCC and AOCC results are compared with the CTMC results of Wang *et al.* [7].

manifolds, separately. In the case of the singlet manifold, the collision system in its approaching stage evolves along the $4\,^1\Sigma$ state, which is coupled with the $3\,^1\Sigma$ state [asymptotically correlating to the $Si^{2+}(3p^2\ [^1D]) + H^+$ configuration] by a strong Landau-Zener coupling at 11.45 a.u. This coupling is very narrow and sharp and can be treated as diabatic in the high-energy region. During the further evolution of the system toward the united atom region, it evolves (with well-defined probabilities) along the $3\,^1\Sigma$ and $4\,^1\Sigma$ states (mainly the $3\,^1\Sigma$ state at high energy). At about 6.2 a.u., the $3\,^1\Sigma$ state strongly coupled with the $2\,^1\Sigma$ [asymptotically correlating to the $Si^{2+}(3s3p) + H^+$ configuration]; see Figs. 1(a) and 2(a). At small internuclear distances, these states are radially coupled with the $1\,^1\Sigma$ and $5\,^1\Sigma$ states and rotationally coupled with the $^1\Pi$ states. In the receding stage of the collision, the system undergoes the $2\,^1\Sigma$-$3\,^1\Sigma$ and $3\,^1\Sigma$-$4\,^1\Sigma$ couplings again. The $5\,^1\Sigma$ state would undergo the series of strong $5\,^1\Sigma$-$6\,^1\Sigma$-$7\,^1\Sigma$-$8\,^1\Sigma$-$9\,^1\Sigma$ radial couplings at 2.5–8.5 a.u. [see Fig. 1(a)] and promote the system to the $Si^{2+}(3p^2\ [^1S]) + H^+$, $Si^{2+}(3s3d) + H^+$, $Si^{2+}(3s4l) + H^+$ states as well as the $Si^{3+}(3p) + H$ state. The asymptotically degenerate states (such as $2\,^1\Sigma$ and $1\,^1\Pi$ states, $3\,^1\Sigma$ and $2\,^1\Pi$ states) would also undergo the strong rotational couplings even at large internuclear distances. These couplings would only influence the rearrangement of the system between these states.

For the triplet manifold, the entrance channel is the $2\,^3\Sigma$ state. In the approaching stage of the collision, the $2\,^3\Sigma$ initial state exerts a Demkov coupling at $R \approx 5$ a.u. with the $1\,^3\Sigma$ state, which asymptotically correlates to the $Si^{2+}(3s3p) + H^+$ state. During the further evolution, the $2\,^3\Sigma$ state is coupled with the $3\,^3\Sigma$ state at about 3 a.u. At small internuclear distances, the $1\,^3\Sigma$, $2\,^3\Sigma$, and $3\,^3\Sigma$ states rotationally coupled with the $^3\Pi$ states. In the receding stage of the collision, the $2\,^3\Sigma$ state undergoes the $2\,^3\Sigma$-$3\,^3\Sigma$ couplings again. The system is promoted to the $Si^{2+}(3s3d) + H^+$ and $Si^{2+}(3s4l) + H^+$ states as well as the $Si^{3+}(3p) + H$ state by the strong series of $3\,^3\Sigma$-$4\,^3\Sigma$-$5\,^3\Sigma$-$6\,^3\Sigma$ radial couplings at 2.5–8 a.u. Because the $1\,^3\Sigma$-$2\,^3\Sigma$ radial coupling is weaker and appears at a relatively smaller internuclear distance than

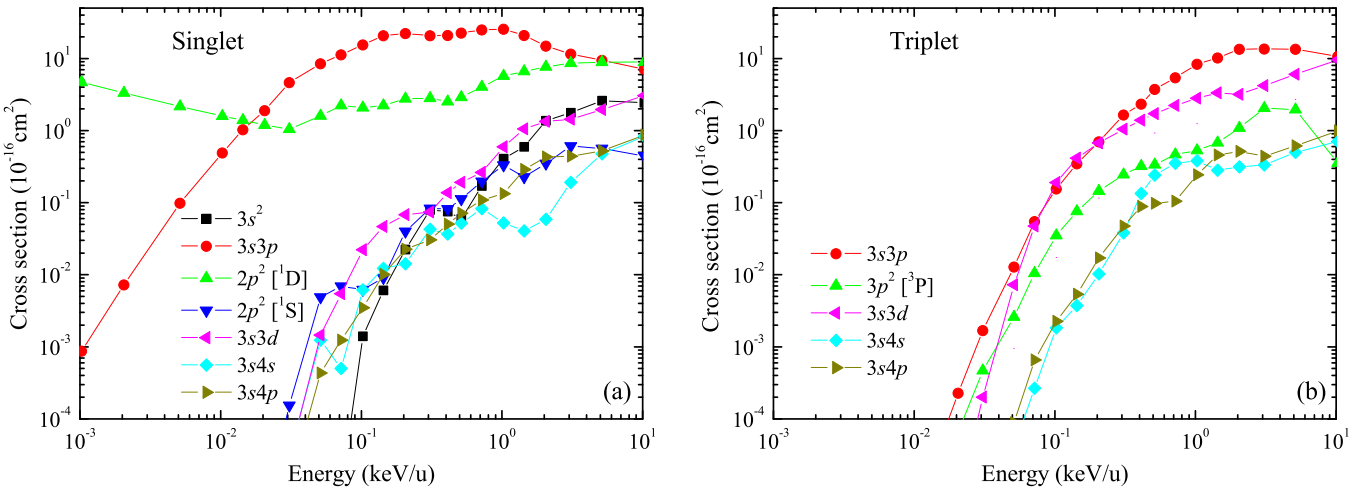

FIG. 7. (Color online) State-selective electron capture cross sections of singlet (a) and triplet (b) states for Si^{3+} + H collision.

the $2\,^1\Sigma$-$3\,^1\Sigma$ coupling, the triplet capture cross sections decrease rapidly at $E < 1$ keV/u.

IV. CONCLUSION

In the present paper we have calculated the total and state-selective electron capture cross sections for the $Si^{3+}(3s)$ + H$(1s)$ collision by using the MOCC and AOCC methods in the energy range of 10^{-5}–10 keV/u and 0.8–200 keV/u, respectively. The molecular data are calculated by the *ab initio* MRDCI package.

The present MOCC electron capture cross sections agree well with the experimental measurements of Bruhns *et al.* [9] in the energy range 0.3–2 keV/u, and at lower energies, the calculated results are larger than the experimental ones. The smaller experimental cross sections of [9] in the low-energy region may be due to the loss of collected signal. Our AOCC calculations agree well with the experiments of Kim *et al.* [8] at 50–150 keV/u. Our MOCC result is in good mutual agreement with the AOCC result at $E = 10$ keV/u. Because of the use of single-electron approximation, the present AOCC calculation would be invalid in the lower-energy region for this collision system. Our MOCC results are larger than the MOCC calculations of Wang *et al.* [7] at $E > 0.04$ keV/u. This is because the rotational couplings involved in the present calculation play very important roles for electron capture. At $E < 10$ eV/u, the present results are three to five times smaller than those in Ref. [7] due to the difference in the molecular data calculation at large internuclear distances. The discrepancies between the present results and the END calculations of Guevara *et al.* [10] at low energies may be attributed to their classical treatment for the nuclear trajectories. The electron capture to the $3s3p$ state dominates the capture process in the energy range of 20 eV/u–20 keV/u. The $3p^2$ state becomes the dominant capture channel at $E < 10$ keV/u. At $E > 20$ keV/u, the $3s3d$ state is also important because it has three compositions. The collision dynamics for both singlet and triplet manifolds are discussed in terms of the most important reaction paths and the involved radial and rotational couplings.

ACKNOWLEDGMENTS

This work was supported by the National Basic Research Program of China (973 Program, Grant No. 2013CB922200), by the National Natural Science Foundation of China (Grants No. 11025417, No. 11204017, and No. 11004014) and by the Foundation for the Development of Science and Technology of the Chinese Academy of Engineering Physics (Grant No. 2012B0102015).

[1] R. K. Janev, L. P. Presnyakov, and V. P. Shevelko, *Physics of Highly Charged Ions* (Springer, Berlin-Heidelberg, 1985).

[2] S. I. Krasheninnikov, A. Yu. Pgarov, and D. J. Sigmar, Phys. Lett. A **214**, 285 (1996); A. Yu. Pgarov and S. I. Krasheninnikov, *ibid.* **222**, 251 (1996).

[3] R. K. Janev, T. Kato, and J. G. Wang, Phys. Plasmas **7**, 4364 (2000).

[4] J. B. Kingdon and G. J. Ferland, Astrophys. J. Lett. **516**, L107 (1999); Astrophys. J., Suppl. Ser. **106**, 205 (1996).

[5] T. E. Cravens, Geophys. Res. Lett. **24**, 105 (1997).

[6] B. Herrero, I. L. Cooper, and A. S. Dickinson, J. Phys. B **29**, 5583 (1996).

[7] J. G. Wang, B. He, Y. Ning, C. L. Liu, J. Yan, P. C. Stancil, and D. R. Schultz, Phys. Rev. A **74**, 052709 (2006).

[8] H. J. Kim, R. A. Phaneuf, F. W. Meyer, and P. H. Stelson, Phys. Rev. A **17**, 854 (1978).

[9] H. Bruhns, H. Kreckel, D. W. Savin, D. G. Seely, and C. C. Havener, Phys. Rev. A **77**, 064702 (2008).

[10] N. L. Guevara, E. Teixeira, B. Hall, Y. Öhrn, E. Deumens, and J. R. Sabin, Phys. Rev. A **83**, 052709 (2011).

[11] B. H. Bransden and M. R. C. McDowell, *Charge Exchange and the Theory of Ion-Atom Collisions* (Clarendon Press, Oxford, 1992).
[12] B. Zygelman, D. L. Cooper, M. J. Ford, A. Dalgarno, J. Gerratt, and M. Raimondi, Phys. Rev. A **46**, 3846 (1992).
[13] R. J. Buenker and R. A. Phillips, J. Mol. Struct.: THEOCHEM **123**, 291 (1985).
[14] S. Krebs and R. J. Buenker, J. Chem. Phys. **103**, 5613 (1995).
[15] T. H. Dunning, Jr., J. Chem. Phys. **90**, 1007 (1989).
[16] G. Hirsch, P. J. Bruna, R. J. Buenker, and S. D. Peyerimhoff, Chem. Phys. **45**, 335 (1980).
[17] M. C. Bacchus-Montabonel and P. Ceyzeriat, Phys. Rev. A **58**, 1162 (1998).
[18] M. Gargaud, R. McCarroll, and P. Valiron, J. Phys. B **20**, 1555 (1987).
[19] W. R. Thorson and J. B. Delos, Phys. Rev. A **18**, 135 (1978).
[20] M. H. Mittleman, Phys. Rev. **188**, 221 (1969).
[21] L. F. Errea, L. Méndez, and A. Riera, J. Phys. B **15**, 101 (1982).
[22] B. R. Johnson, J. Comput. Phys. **13**, 445 (1973).
[23] T. G. Heil, S. E. Butler, and A. Dalgarno, Phys. Rev. A **23**, 1100 (1981).
[24] W. Fritsch and C. D. Lin, Phys. Rep. **202**, 1 (1991).
[25] Yu. Ralchenko and A. E. Kramida, J. Reader, and NIST ASD Team, NIST Atomic Spectra Database (version 3.1.5), 2008, http://physics.nist.gov/asd3.
[26] S. E. Butler and A. Dalgarno, Astrophys. J. **241**, 838 (1980).